NANO LETTERS

Letter

pubs.acs.org/NanoLett

A Broadband, Background-Free Quarter-Wave Plate Based on Plasmonic Metasurfaces

Nanfang Yu,[†,⊥] Francesco Aieta,[†,‡,⊥] Patrice Genevet,[†,§,⊥] Mikhail A. Kats,[†] Zeno Gaburro,[†,∥] and Federico Capasso*[,†]

[†]School of Engineering and Applied Sciences, Harvard University, Cambridge, Massachusetts 02138, United States

[‡]Dipartimento di Scienze e Ingegneria della Materia, dell'Ambiente ed Urbanistica, Università Politecnica delle Marche, via Brecce Bianche, 60131 Ancona, Italy

[§]Institute for Quantum Studies and Department of Physics, Texas A&M University, College Station, Texas 77843, United States

[∥]Dipartimento di Fisica, Università degli Studi di Trento, via Sommarive 14, 38100 Trento, Italy

S *Supporting Information*

ABSTRACT: We demonstrate optically thin quarter-wave plates built with metasurfaces that generate high-quality circularly polarized light over a broad wavelength range for arbitrary orientation of the incident linear polarization. The metasurface consists of an array of plasmonic antennas with spatially varying phase and polarization responses. Experimentally demonstrated quarter-wave plates generate light with a high degree of circular polarization (>0.97) from $\lambda = 5$ to 12 μm, representing a major advance in performance compared to previously reported plasmonics-based wave plates.

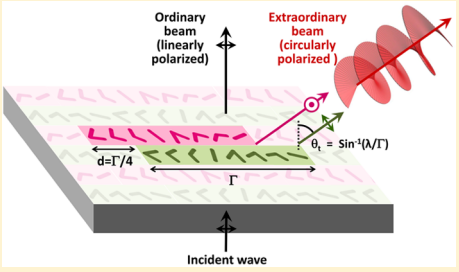

KEYWORDS: *Plasmonics, optical antenna, metasurface, wave plate, broadband*

Considerable attention has been drawn to the properties of anisotropic metallic and dielectric structures, which can mimic the polarization-altering characteristics of naturally occurring birefringent and chiral media. Subwavelength gratings introduce form birefringence[1] and have been used to make quarter-wave plates for infrared and submillimeter waves.[2,3] Planar chiral metasurfaces change the polarization state of transmitted light.[4−9] Circular polarizers based on three-dimensional chiral metamaterials primarily pass light of circular polarization of one handedness, while the transmission of light of the other handedness is suppressed (circular dichroism).[10,11] Because of the difficulty of fabricating thick chiral metamaterials, the demonstrated suppression ratio between circular polarizations of different handedness is quite small (<10). One way to overcome this difficulty is to use planar structures comprising strongly scattering anisotropic particles that are able to abruptly change the polarization of light. Light scattered from such particles changes polarization because the particles have different spectral responses along the two principle axes.[12−23] For example, planar plasmonic wave plates have been created using arrays of identical rod or aperture metallic antennas[24−30] or meander-line structures.[31−33] These types of quarter-wave plates are designed by controlling the spectral responses of the plasmonic eigenmodes so their scattered waves have equal amplitudes and a $\pi/2$ phase difference at the excitation wavelength. This is achieved, for example, by tuning the length of orthogonally oriented dipolar antennas,[24−30] or by adjusting the inductive and capacitive impedance along the two axes of the meander-line structures.[31−33]

These planar wave plates have a number of shortcomings. For example, their bandwidth is limited because of the relatively narrow resonance of the plasmonic eigenmodes. Once the structures operate away from the optimal wavelength, the amplitude ratio R between the two eigenmodes deviates from unity, and their differential phase Ψ is no longer $\pi/2$ (Figure 1a). Another limitation is that the performance of plasmonic wave plates is usually degraded by the optical background that originates from direct transmission through the empty space around the metallic structures (e.g., cross antennas or meander-lines).

In this Letter we have realized metasurfaces based on phased antenna arrays that generate scattered light waves with arbitrary polarization states. In particular, we demonstrated a quarter-wave plate that features ultrabroadband and background free performance and works for any orientation of the incident linear polarization. We have previously used metasurfaces consisting of phased antennas to demonstrate generalized laws of reflection and refraction[34,35] and to generate optical vortex beams.[36] Note that our metasurfaces were designed to operate in the mid-infrared wavelength range, where we primarily use plasmonic effects associated with geometry instead of those associated with the intrinsic properties of metals.

Received: September 15, 2012
Revised: November 3, 2012
Published: November 6, 2012

   dx.doi.org/10.1021/nl303445u | *Nano Lett.* 2012, 12, 6328−6333

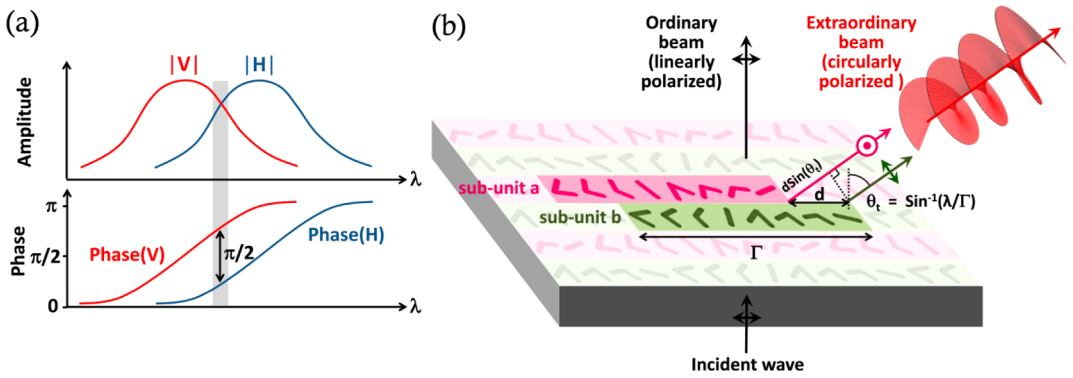

Figure 1. (a) Conventional plasmonic quarter-wave plates are based on arrays of identical anisotropic plasmonic structures that support two orthogonal plasmonic eigenmodes, **V** and **H**, which have an amplitude and phase response characteristic of any resonance (red and blue curves). The devices operate as quarter-wave plates only within a narrow wavelength range (gray area) in which the two eigenmodes have approximately equal scattering amplitudes and a phase difference of $\Psi = \pi/2$. The design also suffers from the presence of a background, which occurs because the scattered light from plasmonic structures is not spatially separated from the directly transmitted light. (b) To circumvent the problems of optical background and narrow bandwidth, we use a different design based on optical antenna metasurfaces. The unit cell of the metasurface consists of two subunits (pink and green), each containing eight gold V-shaped antennas. Upon excitation by linearly polarized incident light, the subunits generate two copropagating waves with equal amplitudes, orthogonal linear polarizations, and a $\pi/2$ phase difference (when offset $d = \Gamma/4$), which produce a circularly polarized extraordinary beam that bends away from the surface normal. The amplitudes of the waves scattered from the two subunits are equal because corresponding antennas in the subunits have the same geometries (i.e., arm length and opening angle); the orthogonal polarizations are ensured by different antenna orientations in the subunits; the $\pi/2$ phase difference is introduced by the offset, d, between the subunits. The metasurface also generates an ordinary beam propagating normal to the surface and polarized in the same way as the incident light.

The schematic of our metasurface quarter-wave plate is shown in Figure 1b. The unit cell consists of two subunits (pink and green in Figure 1b), which generate two copropagating waves with equal amplitudes, orthogonal polarizations, and a $\pi/2$ phase difference. The waves coherently interfere, producing a circularly polarized extraordinary beam that bends away from the propagation direction of the ordinary beam (Figure 1b). Due to the spatial separation of the two beams, the extraordinary beam is background-free. Our quarter-wave plate performs well over a much larger wavelength range compared to existing designs for two reasons. First, the V-antennas have a much broader effective resonance over which the antenna scattering efficiency is significant and the phase response is approximately linear (Figure 2a). This broadened resonance is a result of the combined responses of the two eigenmodes of the V-antennas.[37] Second, our metasurfaces are robust against wavelength change because we use a "balanced" design featuring two subunits in one unit cell. Away from the optimal operating wavelength, the phase and amplitude responses of the array antennas will deviate from their designed values (Figure 2b); nevertheless, the two waves scattered from the two subunits have the same wavefronts (Figure 2b) so they always contribute equally to the extraordinary beam, resulting in a pure circular polarization state.

The basic elements in our metasurface design are gold V-shaped antennas. Each antenna supports symmetric and antisymmetric eigenmodes, which are excited by the components of the incident electric field polarized parallel and perpendicular to the symmetry axis of the V-structure, respectively (Figure 2a, insets).[34,37,38] For arbitrary incident polarization, both modes are excited and contribute to the antenna scattering response. The scattered waves from the eight antennas in a subunit can be written as (see the Supporting Information for derivation):

$$\begin{pmatrix}\vec{\mathbf{E}}_1\\ \vec{\mathbf{E}}_2\\ \vec{\mathbf{E}}_3\\ \vec{\mathbf{E}}_4\\ \vec{\mathbf{E}}_5\\ \vec{\mathbf{E}}_6\\ \vec{\mathbf{E}}_7\\ \vec{\mathbf{E}}_8\end{pmatrix} = \frac{1}{2}\begin{bmatrix}\mathbf{S}_1-\mathbf{A}_1\\ \mathbf{S}_2-\mathbf{A}_2\\ \mathbf{S}_3-\mathbf{A}_3\\ \mathbf{S}_4-\mathbf{A}_4\\ -(\mathbf{S}_1-\mathbf{A}_1)\\ -(\mathbf{S}_2-\mathbf{A}_2)\\ -(\mathbf{S}_3-\mathbf{A}_3)\\ -(\mathbf{S}_4-\mathbf{A}_4)\end{bmatrix}[\cos(2\beta-\alpha)\hat{\mathbf{y}}+\sin(2\beta-\alpha)\hat{\mathbf{x}}] + \frac{1}{2}\begin{pmatrix}\mathbf{S}_1+\mathbf{A}_1\\ \mathbf{S}_2+\mathbf{A}_2\\ \mathbf{S}_3+\mathbf{A}_3\\ \mathbf{S}_4+\mathbf{A}_4\\ \mathbf{S}_1+\mathbf{A}_1\\ \mathbf{S}_2+\mathbf{A}_2\\ \mathbf{S}_3+\mathbf{A}_3\\ \mathbf{S}_4+\mathbf{A}_4\end{pmatrix}(\cos\alpha\hat{\mathbf{y}}+\sin\alpha\hat{\mathbf{x}}) \quad (1)$$

Here α and β are the orientation angles of the incident field and the antenna symmetry axis, respectively; $\hat{\mathbf{x}}$ and $\hat{\mathbf{y}}$ are the unit vectors along the x- and y-axes, respectively (Figures 3a and b); $\mathbf{S}_i$ and $\mathbf{A}_i$ are the complex scattering amplitudes of the symmetric and antisymmetric mode of the ith antenna in the subunit, respectively (Figure 2a). Equation 1 shows that the scattered light from the antennas ($\vec{\mathbf{E}}_i$, with $i = 1-8$) contains two terms, which are polarized along the $(2\beta-\alpha)$-direction and the α-direction from the y-axis, respectively. The antenna array is designed so that at $\lambda = 8$ μm the $(2\beta-\alpha)$-polarized components of all of the antennas have the same amplitude and

dx.doi.org/10.1021/nl303445u | Nano Lett. 2012, 12, 6328−6333

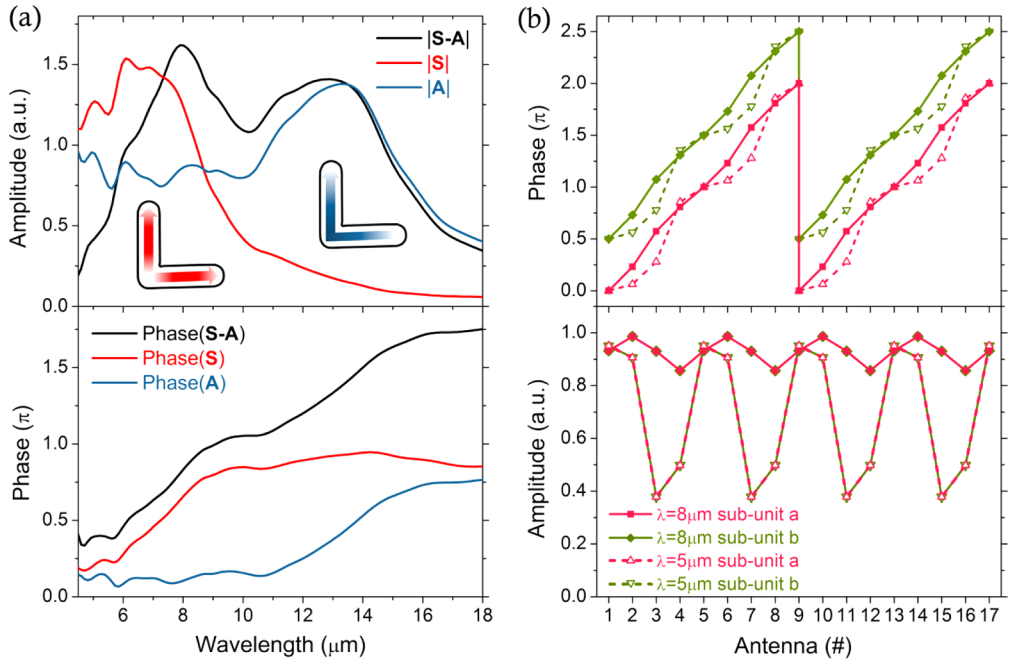

Figure 2. (a) Amplitude and phase responses of **S**, **A**, and **S**−**A** for a representative V-antenna obtained by full-wave simulations; here **S** and **A** represent the complex scattering amplitudes of the symmetric and antisymmetric eigenmodes, respectively.[34,37,38] The arm length of the V-antenna is 1.13 μm and the angle between the two arms is 90°. This is the second antenna from the left in a given subunit (Figure 3a). The two current eigenmodes of the antenna are shown in the insets. The arrows refer to the direction of current flow, and the colors represent current density, with darker colors representing larger currents. The scattered light from the antenna can be decomposed into two components (**S** + **A**) and (**S** − **A**). By properly designing the phase and amplitude responses of these components in the antenna arrays, we can spatially separate them so that (**S** + **A**) and (**S** − **A**) lead to, respectively, the ordinary and extraordinary beams propagating in different directions. Because of the much broader effective plasmonic resonance as a result of the combined responses (i.e., **S** − **A** as compared to **S** or **A**), our metasurface quarter-wave plates can provide significant scattering efficiency over a broader wavelength range, as is shown in the upper panel of a. The combined plasmonic resonances can also provide a larger coverage in the phase response (i.e., ~1.5π for **S** − **A** as compared to ~0.75π for **S** or **A**), as is shown in the lower panel of a. (b) Calculated phase and amplitude responses along the antenna array. Responses for two consecutive subunits are shown (i.e., antennas 9−16 are identical to antennas 1−8). Pink and green curves are for the first and second subunits, respectively; solid and dashed curves are for excitation wavelengths of 8 and 5 μm, respectively. As designed, the phase response at λ = 8 μm exhibits an almost constant gradient (i.e., 2π over 8 antennas in the subunit); the amplitude response at this wavelength is quite uniform. These properties correspond to an extraordinary beam with a flat wavefront and high intensity. However, at λ = 5 μm the phase response does not follow a perfect linear profile, and the amplitude response shows large variations. Even in this nonideal situation, however, one still obtains an extraordinary beam with close-to-unity degree of circular polarization (but with reduced intensity) because the waves scattered from the two subunits always give equal contributions to the beam since they have exactly the same wavefronts (compare the dashed curves in the upper and lower panel of b).

an incremental phase of $\Delta\Phi = \pi/4$. That is, $|\mathbf{S}_i - \mathbf{A}_i|$ is constant, with i = 1−4, and **Phase** $(\mathbf{S}_{i+1} - \mathbf{A}_{i+1})$ − **Phase** $(\mathbf{S}_i - \mathbf{A}_i) = \pi/4$, with i = 1−3 (Figure 2b). Therefore the $(2\beta-\alpha)$-polarized partial waves scattered from the antenna array produce a wave propagating along the $\theta_t = \arcsin(\lambda/\Gamma)$ direction from the surface normal;[34] here λ is the free-space wavelength, and Γ is the length of the subunit. On the other hand, the α-polarized components, which have the same polarization as the incident light, have unequal amplitudes but similar phase responses (Supporting Information). Therefore, the α-polarized partial waves combine to form a wave that propagates in a direction normal to the metasurface for normally incident light and contributes to the ordinary beam.

The metasurface quarter-wave plate has a unit cell consisting of two subunits that are offset from each other in the horizontal direction by d (Figure 3a). They create two coherent waves that propagate along the $\theta_t = \arcsin(\lambda/\Gamma)$ direction (Figure 1b). The waves spatially overlap since the spacing between the two subunits in the y-direction is much smaller than the free-space wavelength (Figure 3a). The waves have equal amplitudes because the corresponding antennas in the two subunits have the same geometries (i.e., arm length and opening angle of the V-structures). Cross-polarization between the waves is achieved by choosing antenna orientations $\beta_1 = 67.5°$ and $\beta_2 = 112.5°$ so that $(2\beta_2 - \alpha) - (2\beta_1 - \alpha) = 90°$ (Figure 3a and b). The 90° phase difference between the waves as well as the handedness of the circular polarization is controlled by choosing the offset $d = \pm\Gamma/4$, so that $\Psi = k_o d \sin(\theta_t) = 2\pi d/\Gamma = \pm 90°$ (Figure 1b). As a result of these properties, the waves scattered from the two subunits coherently interfere, producing a circularly polarized extraordinary beam (Figure 1b). Note that once $\beta_2 - \beta_1 = 45°$, the two waves will always be cross-polarized, which is independent of the orientation angle α of the linearly polarized incident light.

Our optical antenna arrays can provide phase coverage from 0° to 360° with an increment of ~45° over a wide range of wavelengths (Figure S1(a) in the Supporting Information). Therefore, the metasurface quarter-wave plates can generate well-defined extraordinary beams over a broad spectral range. Figure 3c shows experimental far-field scans at excitation wavelengths from 5.2 to 9.9 μm. Three samples with Γ = 13, 15, and 17 μm have been tested. For all samples and excitation wavelengths, we observe the ordinary and extraordinary beams and negligible optical background. The observed angular

dx.doi.org/10.1021/nl303445u | Nano Lett. 2012, 12, 6328−6333

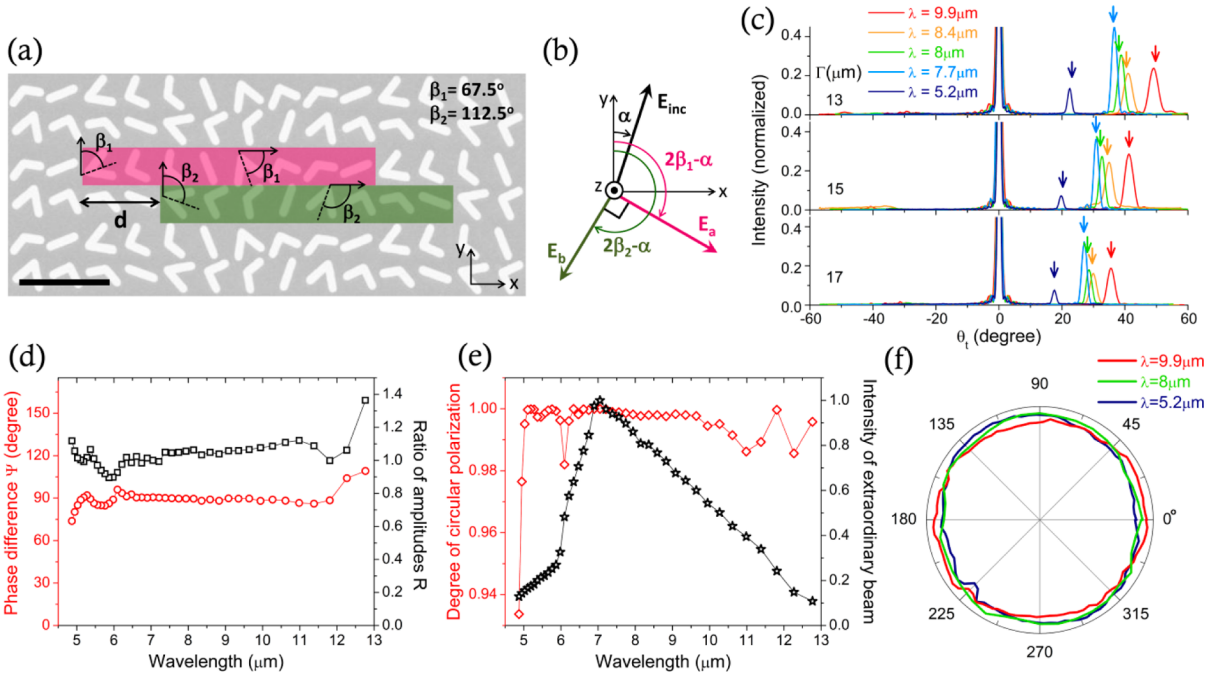

Figure 3. (a) Scanning electron microscope (SEM) image of a metasurface quarter-wave plate. The unit cell of the metasurface comprises two subunits (pink and green). Each subunit contains eight V-antennas, with the last four antennas obtained by rotating the first four clockwise by 90°. Antenna orientation angles are indicated by β_1 and β_2, and dashed lines represent the antenna symmetry axes. The scale bar is 4 μm. Shown is a small portion of the wave plate. The entire antenna array has a footprint of 230 × 230 μm^2 to accommodate the plane-wave like incident light. (b) Schematic showing the polarization of the two waves $\mathbf{E}_a$ and $\mathbf{E}_b$ scattered from the two subunits, as well as that of the incident light. (c) Experimental far-field scans showing extraordinary beams at $\theta_t > 0$ generated by metasurfaces with different interfacial phase gradients (from $2\pi/13$ μm to $2\pi/17$ μm) at different wavelengths (from 5.2 to 9.9 μm), as well as the ordinary beams located at $\theta_t = 0$, given normally incident excitation. Here the incident polarization is along y-axis ($\alpha = 0°$). The scans are normalized with respect to the intensity of the ordinary beams. At a wavelength of 7.7 μm, the intensity of the extraordinary beams is 30−40% of that of the ordinary beams, corresponding to ∼10% of the total incident power. The arrows indicate the calculated angular positions of the extraordinary beams according to $\theta_t = \arcsin(\lambda/\Gamma)$. (d) Calculated phase difference Ψ and ratio of amplitudes R between the two waves $\mathbf{E}_a$ and $\mathbf{E}_b$ as a function of wavelength. (e) Calculated degree of circular polarization and intensity of the extraordinary beam as a function of wavelength. (f) State-of-polarization analysis for the extraordinary beam at λ = 5.2, 8, and 9.9 μm. The measurements are performed by rotating a linear polarizer in front of a detector and measuring the transmitted power. The incident polarization is oriented at an angle $\alpha = 0°$ (see part b).

positions of the extraordinary beams agree very well with the generalized law of refraction in the presence of the interfacial phase gradient, $\theta_t = \arcsin(\lambda/\Gamma)$ (Figure 3c). At 8 μm, close to the optimal operating wavelength, our metasurfaces scatter approximately 10% of the incident light into the extraordinary beam. The power dissipated in the antenna structures due to absorption is about 10% of the incident power.

Figure 3d shows the phase difference Ψ and amplitude ratio R between the two waves scattered from the subunits, as calculated via full-wave numerical simulations using the finite difference time domain (FDTD) method. It is observed that Ψ and R are in the close vicinity of 90° and 1, respectively, over a wide wavelength range from λ = 5 to 12 μm; correspondingly, a high degree of circular polarization (DOCP) close to unity can be maintained over the wavelength range (Figure 3e). Here DOCP is defined as $|I_{RCP} - I_{LCP}|/|I_{RCP} + I_{LCP}|$, where I_{RCP} and I_{LCP} stand for the intensities of the right and left circularly polarized components in the extraordinary beam, respectively.[33] We observed in experiments that the extraordinary beam is circularly polarized with high purity between λ = 5 and 10 μm (Figure 3f). The experimentally demonstrated suppression ratio between I_{RCP} and I_{LCP} is ∼500, 700, and 400 at λ = 9.9, 8, and 5.2 μm, respectively. The extraordinary beam reaches its peak intensity at $\lambda \approx 7$ μm (Figure 3e). The intensity decreases toward longer and shorter wavelengths because the **S**−**A** components of the scattered light from the antenna arrays start to have mismatched amplitudes and a nonlinear phase distribution. We define the bandwidth of a quarter-wave plate $\Delta\lambda_{qw}$ as the wavelength range over which DOCP is sufficiently close to 1 (e.g., >0.95) and an output with high intensity can be maintained (e.g., intensity larger than half of the peak value). According to this definition, the bandwidth of our metasurface quarter-wave plates is about 4 μm (i.e., from $\lambda \approx 6$ to 10 μm; see Figure 3e), which is about 50% of the central operating wavelength $\lambda_{central}$.

We have verified that the intensity and propagation direction of the extraordinary beam is independent of the orientation of the incident linear polarization (Figure 4a). The extraordinary beam maintains a high DOCP when the incident polarization changes (Figure 4b). The polarizations of the waves scattered from the two subunits are controlled by angles α, β_1, and β_2 and their amplitudes are controlled by the scattering amplitudes, **S** and **A**, of the antenna eigenmodes (eq 1). This decoupling between polarization and amplitude allows us to synthesize beams with arbitrary polarization states. In addition to circularly polarized beams (Figure 3), we were able to generate elliptically polarized extraordinary beams by simply changing the subunit offset d (Figure 5). For example, when $d = \Gamma/8$ (or $3\Gamma/8$), the two waves scattered from the subunits have perpendicular polarization, equal amplitudes, and a phase difference of $\Psi = \pi/$

dx.doi.org/10.1021/nl303445u | Nano Lett. 2012, 12, 6328−6333

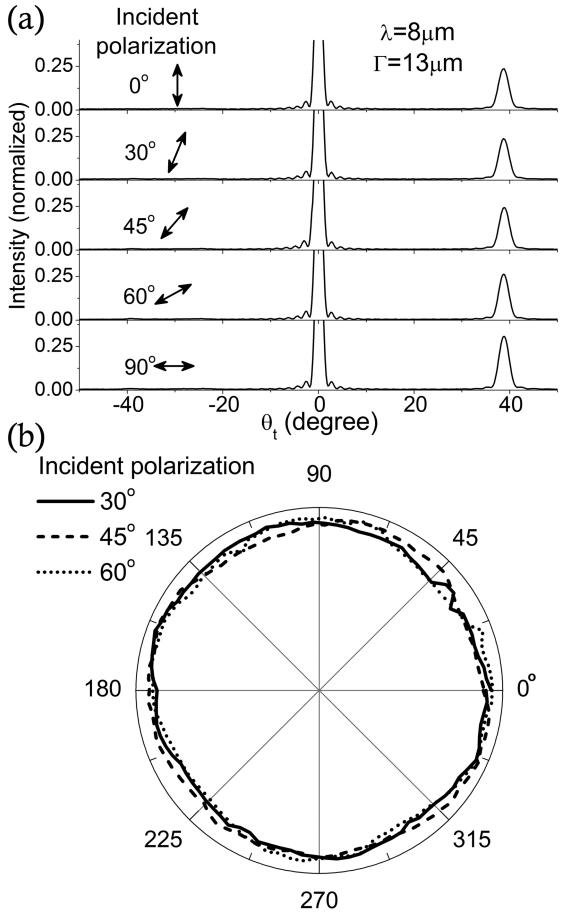

Figure 4. (a) Experimental far-field scans of the ordinary and extraordinary beams generated by a metasurface quarter-wave plate for different incident polarizations. (b) State-of-polarization analysis for the extraordinary beam at three different incident polarizations.

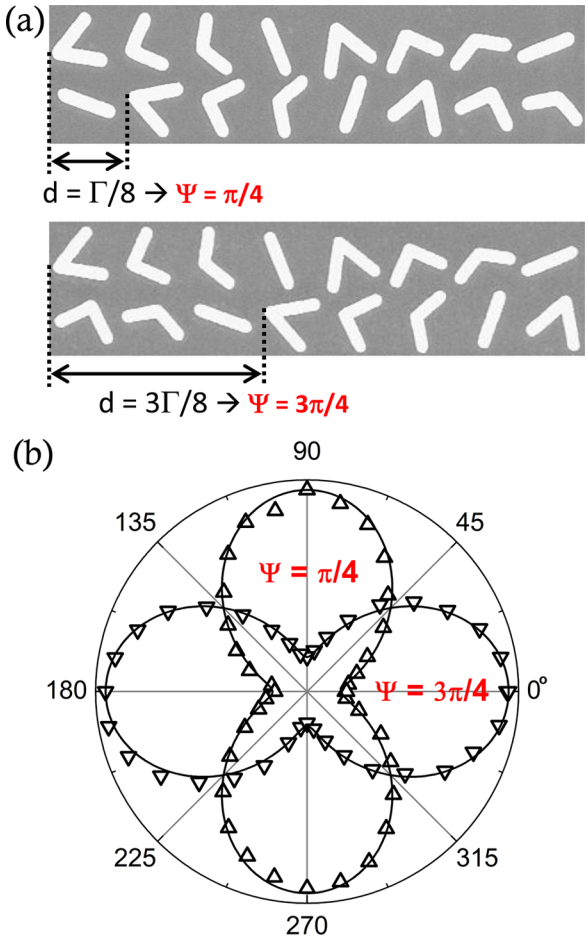

Figure 5. The offset between the subunits, d, controls the phase difference between the waves scattered from the two subunits and therefore the polarization of the extraordinary beam. The phase difference is $\Psi = k_o d \sin(\theta_t) = 2\pi d/\Gamma$. Therefore, $d = \Gamma/4$ will lead to circular polarization, shown in Figure 3; elliptical polarization states corresponding to $\Psi = \pi/4$ and $3\pi/4$ are shown in this figure. (a) SEM images of the unit cells. (b) Results of the state-of-polarization analysis. The incident polarization is oriented at an angle $\alpha = 0°$ (see Figure 3b). The symbols are measurements, and the curves are analytical calculations assuming that the two scattered waves have equal amplitudes and a phase difference equal to the value of Ψ indicated in the figure.

4 (or $3\pi/4$), thus forming an elliptically polarized beam. The state-of-polarization analysis of the beam shown in Figure 5b is in good agreement with analytical calculations.

Our metasurface design has a few limitations. First, it is inherently dispersive. The circularly polarized extraordinary beams created at different wavelengths propagate in different directions according to $\theta_t = \arcsin(\lambda/\Gamma)$. Second, the efficiency of the metasurface quarter-wave plate is not high. In addition to the circularly polarized extraordinary beam in transmission, which carries about 10% of the incident power, there are ordinary reflection and refraction, as well as a second extraordinary beam in reflection created by the phased antenna array. The efficiency can be increased by using denser antenna arrays or by exploiting antenna designs with higher scattering amplitude. For example, reflect-array structures consisting of phased antennas separated by a dielectric spacing layer from a metallic back plane are able to shape the wavefront of reflection with high efficiency.[39]

Wave plates are some of the most ubiquitous components in optics. Most commonly used designs are based on bulk birefringent crystals with optical anisotropy. This conventional approach has several limitations: it is relatively narrow band, and it relies on the availability of birefringent materials in the desired frequency range. Approaches exist to overcome the latter limitation, which utilize form birefringence of anisotropic structures such as plasmonic antennas. These come with their own limitations; in particular, they exhibit relatively low purities of polarization and often superimpose an optical background onto the desired signal. In addition, the bandwidth of these devices is also relatively small. Our approach, which involves *spatially inhomogeneous* arrays of anisotropic optical antennas, overcomes many of these limitations. We experimentally demonstrated quarter-wave plates, which are broadband and feature high polarization purity (e.g., output with DOCP larger than 0.97 over $\lambda = 5$ to 12 μm, and with intensity larger than half-maximum over $\lambda = 6$ to 10 μm). This approach requires only a single step of conventional lithography and is generalizable from the visible to the radio frequency regimes.

■ ASSOCIATED CONTENT

Supporting Information

Fabrication, derivation of the scattered waves from the eight antennas, broadband performance of V-antennas, Table 1, and

dx.doi.org/10.1021/nl303445u | *Nano Lett.* 2012, 12, 6328−6333

Figure S1. This material is available free of charge via the Internet at http://pubs.acs.org.

AUTHOR INFORMATION

Corresponding Author

*E-mail: capasso@seas.harvard.edu.

Author Contributions

⊥These authors contributed equally to this work.

Notes

The authors declare no competing financial interest.

ACKNOWLEDGMENTS

The authors acknowledge support from the National Science Foundation, Harvard Nanoscale Science and Engineering Center (NSEC) under contract NSF/PHY 06-46094, and the Center for Nanoscale Systems (CNS) at Harvard University. This work was supported in part by the Defense Advanced Research Projects Agency (DARPA) N/MEMS S&T Fundamentals program under Grant N66001-10-1-4008 issued by the Space and Naval Warfare Systems Center Pacific (SPAWAR). P.G. acknowledges funding from the Robert A. Welch Foundation (A-1261). Z.G. acknowledges funding from the European Communities Seventh Framework Programme (FP7/2007-2013) under Grant PIOF-GA-2009-235860. M.A.K. is supported by the National Science Foundation through a Graduate Research Fellowship. Harvard CNS is a member of the National Nanotechnology Infrastructure Network (NNIN).

REFERENCES

(1) Born, M.; Wolf, E. *Principles of Optics*, 7th ed.; Cambridge University Press: Cambridge, 1999.
(2) Kikuta, H.; Ohira, Y.; Iwata, K. *Appl. Opt.* **1997**, *36*, 1566−1572.
(3) van Vliet, A. H. F.; de Graauw, Th. *Int. J. Infrared Millimet. Waves* **1981**, *2*, 465−477.
(4) Papakostas, A.; Potts, A.; Bagnall, D. M.; Prosvirnin, S. L.; Coles, H. J.; Zheludev, N. I. *Phys. Rev. Lett.* **2003**, *90*, 107404.
(5) Prosvirnin, S. L.; Zheludev, N. I. *Phys. Rev. E* **2005**, *71*, 037603.
(6) Plum, E.; Zhou, J.; Dong, J.; Fedotov, V. A.; Koschny, T.; Soukoulis, C. M.; Zheludev, N. I. *Phys. Rev. B* **2009**, *79*, 035407.
(7) Zhang, S.; Park, Y.-S.; Li, J.; Lu, X.; Zhang, W.; Zhang, X. *Phys. Rev. Lett.* **2009**, *102*, 023901.
(8) Xiong, X.; Sun, W.-H.; Bao, Y.-J.; Wang, M.; Peng, R.-W.; Sun, C.; Lu, X.; Shao, J.; Li, Z.-F.; Ming, N.-B. *Phys. Rev. B* **2010**, *81*, 075119.
(9) Decker, M.; Zhao, R.; Soukoulis, C. M.; Linden, S.; Wegener, M. *Opt. Lett.* **2010**, *35*, 1593−1595.
(10) Gansel, J. K.; Thiel, M.; Rill, M. S.; Decker, M.; Bade, K.; Saile, V.; von Freymann, G.; Linden, S.; Wegener, M. *Science* **2009**, *325*, 1513−1515.
(11) Zhao, Y.; Belkin, M. A.; Alù, A. *Nat. Commun.* **2012**, *3*, 870.
(12) van de Hulst, H. C. *Light Scattering by Small Particles*; Wiley: New York, 1957.
(13) Heller, W.; Nakagaki, M. *J. Chem. Phys.* **1974**, *61*, 3619−3625.
(14) Svirko, Y.; Zheludev, N. I.; Osipov, M. *Appl. Phys. Lett.* **2001**, *78*, 498−500.
(15) Khlebtsov, N. G.; Melnikov, A. G.; Bogatyrev, V. A.; Dykman, L. A.; Alekseeva, A. V.; Trachuk, L. A.; Khlebtsov, B. N. *J. Phys. Chem. B* **2005**, *109*, 13578−13584.
(16) Yang, H. *J. Phys. Chem. A* **2007**, *111*, 4987−4997.
(17) González, A. L.; Reyes-Esqueda, J. A.; Noguez, C. *J. Phys. Chem. C* **2008**, *112*, 7356−7362.
(18) Gotschy, W.; Vonmetz, K.; Leitner, A.; Aussenegg, F. R. *Opt. Lett.* **1996**, *21*, 1099−1101.
(19) Gryczynski, Z.; Lukomska, J.; Lakowicz, J. R.; Matveeva, E. G.; Gryczynski, I. *Chem. Phys. Lett.* **2006**, *421*, 189−192.
(20) Calander, N.; Gryczynski, I.; Gryczynski, Z. *Chem. Phys. Lett.* **2007**, *434*, 326−330.
(21) Sukharev, M.; Sung, J.; Spears, K. G.; Seideman, T. *Phys. Rev. B* **2007**, *76*, 184302.
(22) Shegai, T.; Li, Z.; Dadosh, T.; Zhang, Z.; Xu, H.; Haran, G. *Proc. Natl. Acad. Sci. U.S.A.* **2008**, *105*, 16448−16453.
(23) Sung, J.; Sukharev, M.; Hicks, E. M.; Van Duyne, R. P.; Seideman, T.; Spears, K. G. *J. Phys. Chem. C* **2008**, *112*, 3252−3260.
(24) Biagioni, P.; Savoini, M.; Huang, J.-S.; Duò, L.; Finazzi, M.; Hecht, B. *Phys. Rev. B* **2009**, *80*, 153409.
(25) Pors, A.; Nielsen, M. G.; Della Valle, G.; Willatzen, M.; Albrektsen, O.; Bozhevolnyi, S. I. *Opt. Lett.* **2011**, *36*, 1626−1628.
(26) Ellenbogen, T.; Seo, K.; Crozier, K. B. *Nano Lett.* **2012**, *12*, 1026−1031.
(27) Elliott, J.; Smolyaninov, I. I.; Zheludev, N. I.; Zayats, A. V. *Phys. Rev. B* **2004**, *70*, 233403.
(28) Gordon, R.; Brolo, A. G.; McKinnon, A.; Rajora, A.; Leathem, B.; Kavanagh, K. L. *Phys. Rev. Lett.* **2004**, *92*, 037401.
(29) Khoo, E. H.; Li, E. P.; Crozier, K. B. *Opt. Lett.* **2011**, *36*, 2498−2500.
(30) Zhao, Y.; Alù, A. *Phys. Rev. B* **2011**, *84*, 205428.
(31) Young, L.; Robinson, L. A.; Hacking, C. A. *IEEE Trans. Antennas Propag.* **1973**, *21*, 376−378.
(32) Strikwerda, A. C.; Fan, K.; Tao, H.; Pilon, D. V.; Zhang, X.; Averitt, R. D. *Opt. Express* **2009**, *17*, 136−149.
(33) Wadsworth, S. L.; Clem, P. G.; Branson, E. D.; Boreman, G. D. *Opt. Mater. Express* **2011**, *1*, 466−479.
(34) Yu, N.; Genevet, P.; Kats, M. A.; Tetienne, J.-P.; Aieta, F.; Capasso, F.; Gaburro, Z. *Science* **2011**, *334*, 333−337.
(35) Aieta, F.; Genevet, P.; Yu, N.; Kats, M. A.; Gaburro, Z.; Capasso, F. *Nano Lett.* **2012**, *12*, 1702−1706.
(36) Genevet, P.; Yu, N.; Aieta, F.; Lin, J.; Kats, M. A.; Blanchard, R.; Scully, M. O.; Gaburro, Z.; Capasso, F. *Appl. Phys. Lett.* **2012**, *100*, 13101.
(37) Kats, M. A.; Genevet, P.; Aoust, G.; Yu, N.; Blanchard, R.; Aieta, F.; Gaburro, Z.; Capasso, F. *Proc. Natl. Acad. Sci. U.S.A.* **2012**, *109*, 12364−12368.
(38) Blanchard, R.; Aoust, G.; Genevet, P.; Yu, N.; Kats, M. A.; Gaburro, Z.; Capasso, F. *Phys. Rev. B* **2012**, *85*, 155457.
(39) Pozar, D. M.; Targonski, S. D.; Syrigos, H. D. *IEEE Trans. Antennas Propag.* **1997**, *45*, 287−296.